metals

MDPI

Article

Effects of Natural Aging and Discontinuous Cyclic Loading on High Cycle Fatigue Behavior of Steels

Gen Li [1], Jiajun Liu [1,2], Jian Sun [1,2] and Chengqi Sun [1,2,*]

[1] State Key Laboratory of Nonlinear Mechanics, Institute of Mechanics, Chinese Academy of Sciences, Beijing 100190, China
[2] School of Engineering Science, University of Chinese Academy of Sciences, Beijing 100049, China
* Correspondence: scq@lnm.imech.ac.cn

Abstract: Metallic components may not be used immediately and are stored for several months or years after fabrication in some cases, which experience long-term natural aging. Moreover, the fatigue-beared components commonly suffer discontinuous cyclic loadings in service. In this paper, the effects of natural aging and discontinuous loading on high cycle fatigue life and failure mechanism were investigated through rotating bending fatigue tests. The long-term natural aging (e.g., more than 20,000 h) reduced the fatigue life of both 25CrMo4 and 30CrMnSiA steels, and this effect was irrespective of the roughness of the specimen surface. The effect of natural aging on the failure mechanism was related to the microstructure of materials. The natural aging promoted the probability of multi-site crack initiation for 25CrMo4 steel, but had no influence on the crack initiation mode of 30CrMnSiA steel. The discontinuous cyclic loading had no harmful influence on the fatigue life of 25CrMo4 steel, and it had no influence on the failure mechanism. The specimens under continuous and discontinuous cyclic loadings both failed from single-site crack initiation or multi-site crack initiation at the specimen surface.

Keywords: natural aging; discontinuous loading; steels; high cycle fatigue; failure mechanism

Citation: Li, G.; Liu, J.; Sun, J.; Sun, C. Effects of Natural Aging and Discontinuous Cyclic Loading on High Cycle Fatigue Behavior of Steels. *Metals* **2023**, *13*, 511. https://doi.org/10.3390/met13030511

Academic Editor: Filippo Berto

Received: 8 February 2023
Revised: 26 February 2023
Accepted: 27 February 2023
Published: 3 March 2023

1. Introduction

Steels used in structures and components of vehicles often work under cyclic loadings, and their high cycle fatigue (HCF) performance could be concerned [1–5]. Many factors influencing the fatigue behavior of steels have been studied in literature, such as stress ratio, loading frequency, thermal aging, environmental corrosion, defects in surface and interior and so on [6–14]. In practical application, the steels and components may not be used instantly after their fabrication, namely that they are stored for a period before their use [15]. In this way, the steels and components experience a natural-aging period, and the effect of natural aging needs to be elucidated.

According to the existing studies [15–18], the effect of natural aging on the mechanical behaviors is diversified for different kinds of steels. Botvina et al. [16] investigated the effect of storage of 15 years on the fatigue behavior of a low carbon steel and found that the fatigue strength decreased obviously after such long-term storage. It was due to corrosion and hydrogen penetration at local regions of the low carbon steel. Li et al. [15] studied the effect of natural aging of 10,000 h (about 14 months) on the very high cycle fatigue (VHCF) behavior of bearing steel GCr15, and the results showed that the natural aging had prolonged the fatigue life of GCr15 steel in VHCF regime. Based on the observation of the microstructure before and after natural aging, such strengthening in fatigue behavior was attributed to more precipitation of granular carbides after natural aging, which strengthened the microstructure of GCr15 steel. Chang [17] and Zamani et al. [18] studied the short-term aging effect (i.e., 20 s to 10^7 s and 7.8×10^5 s, respectively) at room temperature on low carbon dual phase steels, and the results indicated that the aging above 10^4 s at

room temperature contributed to improvement of the tensile strength and the hardness of the material. Based on the observation of microstructures, the enhancement should be attributed to carbon supersaturation of ferrite and formation of fine precipitates in ferrite grains. The variable effects of natural aging have also been observed for aluminum alloys [19–22]. Tai et al. [19] and Fritsch and Wagner [20] studied the effect of natural aging on the mechanical performance of AA7075 aluminum alloy, and found that the hardness and strength of the aluminum alloy increased after longer natural aging due to the strengthening effect of more precipitates in the microstructure during the natural aging. However, the effect of natural aging on the strength of Al-Mg-Si alloy becomes negative [21]. By using the atom probe tomography and transmission electron microscope, it was found that the numerous unstable clusters were formed after longer natural aging and they inhibited the formation of fine precipitates as well as the strengthening of the precipitates. According to these results, influence of the natural aging on different materials is various. The limited understanding of the effect of natural aging on the fatigue performance of steels make it important to study this effect.

Moreover, the steel components in vehicles commonly suffer discontinuous cyclic loadings in service, e.g., the vehicles work for a while and then stop and repeat this process. This loading mode is different from the experimentally applied continuous fatigue loading, and its influence is also worthy of investigation. However, to the authors' knowledge, the related studies of metallic materials subjected to discontinuous cyclic loading are rare. Sun et al. [23] studied the effect of intermittent loading on the dwell fatigue behavior and conventional fatigue behavior of Ti-6Al-4V ELI alloy. They found that the intermittent loading time did not affect the dwell fatigue life and fatigue failure mechanism of the titanium alloy, but it reduced the fatigue life and promoted multi-site crack initiation in the conventional fatigue scenarios. In other studies, intermittent loading was used to prevent heating of specimens in ultrasonic frequency fatigue tests [24,25], or was used to arrest fatigue crack characteristics in fatigue crack propagation tests [26]. Therefore, the effect of discontinuous cyclic loading on the fatigue behavior and failure mechanism of steels needs to be further investigated.

The current research aims to study the effects of natural aging and discontinuous cyclic loading on the HCF behavior of steels. Two kinds of steels were chosen in this study as reference. One is a common low carbon steel 25CrMo4, and the other is a widely used medium carbon structural steel 30CrMnSiA. To view a continuum variation of long-term natural-aging effect, three different conditions of specimens were considered,, i.e., initial state, after the first natural aging period and after the second natural aging period. Moreover, the rotating bending fatigue tests under continuous loading and discontinuous loading were performed for 25CrMo4 specimens to study the effect of intermittent loading. The fatigue life data and fatigue fracture surfaces of these specimens were examined to gain more understanding for these effects.

2. Materials and Experiments

2.1. Materials and Specimens

The low carbon steel 25CrMo4 and medium carbon steel 30CrMnSiA are investigated in this paper, and their chemical compositions are shown in Table 1. The specimens are designed to be an hourglass shape, as shown in Figure 1. The parallel parts and the minimum section have diameters of 10 mm and 3.5 mm, respectively, and the hourglass part has a radius of 7 mm. The 25CrMo4 steel was in an as-received state and had a hardness of 274 kgf/mm^2. The fatigue specimens were machined out from the as-received material and the minimum sections of the fatigue specimens were polished carefully. The 30CrMnSiA steel was heated at 880 °C in a vacuum furnace for 45 min, followed by oil-quenched and tempered at 550 °C in air for 1 h. The heat-treated 30CrMnSiA steel had a hardness of 339 kgf/mm^2. The fatigue specimens were machined out from the heat-treated material and the specimen surfaces were not polished after machining.

Table 1. Chemical compositions of the tested steels.

Materials	Chemical Compositions (wt%)							
25CrMo4	C 0.22	Cr 0.54	Si 0.26	Mn 0.85	Mo 0.17	S 0.027	P 0.016	Fe balanced
30CrMnSiA		C 0.34	Cr 1.20	Mn 1.10	Si 1.10	Fe balanced		

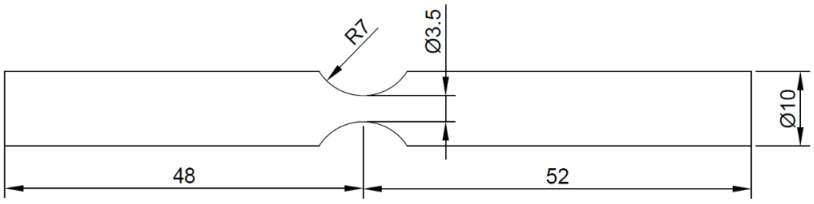

Figure 1. Geometry of specimens for rotating bending fatigue tests (in mm).

2.2. Experimental Methods

Based on the testing standard GB/T 4337-2015 [27], the fatigue tests were conducted on a GIGAQUAD YRB200 rotating bending fatigue machine with a frequency of 50 Hz and stress ratio (R) of -1 at room temperature in air, as shown in Figure 2a. Figure 2b shows the stress diagram of the minimum section of the specimen under bending load. The stress ratio $R = -1$ means that the cyclic loading is fully reversed. According to mechanics of materials [28] and the standard GB/T 4337-2015 [27], the equations to calculate the maximum stress (σ_{max}) is given below.

$$\sigma_{max} = \frac{32FL}{\pi d^3} \quad (1)$$

where F is value of the external load, L is the distance from the acting line of external load to the minimum section, d is the diameter of the minimum section of the specimens.

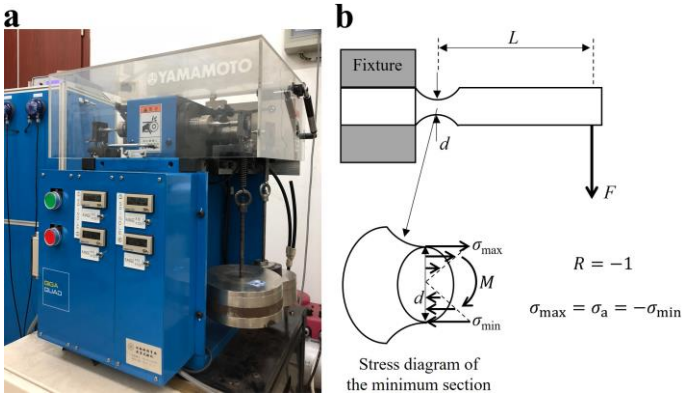

Figure 2. (**a**) GIGAQUAD YRB200 rotating bending fatigue machine. (**b**) A stress diagram of the minimum section of the specimen under bending load.

For the effect of natural aging, the specimens of 25CrMo4 steel were tested in the initial state and after natural-aging periods of 26,000 h (36 months, named NA-26000) and 34,000 h (47 months, named NA-34000), respectively, and the number of the tested specimens were eight, eight, and five, respectively. The specimens of 30CrMnSiA steel were tested in the initial state and after natural-aging periods of 8800 h (12 months, named NA-8800) and 20,000 h (28 months, named NA-20000), respectively, and the number of the tested specimens were three, six and three, respectively. The stress amplitudes of

330 MPa and 580 MPa were determined for the fatigue specimens of 25CrMo4 steel and the 30CrMnSiA steel, respectively.

For the effect of discontinuous cyclic loading, two groups of 25CrMo4 specimens were tested under the stress amplitude of 330 MPa. One group was loaded continuously, and the other was firstly loaded for 1 h and then stopped the machine. When the machine was totally stopped, started the machine immediately and repeated this procedure until failure. The two groups were both from the batch of 25CrMo4 specimens after NA-34000, and each group had five specimens.

The microstructures of the two kinds of steels were observed by an optical microscope. The hardness was measured by a microhardness tester with a load of 25 gf and a holding time of 15 s. After the fatigue tests, the fracture surfaces of the failed specimens were observed by a scanning electron microscope (SEM).

3. Results and Discussion

3.1. Effect of Natural Aging on HCF of 25CrMo4 Steel

Figure 3a shows the fatigue life data of 25CrMo4 specimens in the initial state and after NA-26000 and NA-34000. It was found that the fatigue lives of specimens after NA-26000 and NA-34000 were lower than those in the initial state as a whole. The 50% survival probability and the cumulative probability of the fatigue life data in the initial state and after NA-26000 and NA-34000were calculated to analyze the effect of natural aging. According to Refs. [15,29], the fatigue life data in logarithm in the same testing conditions were assumed to follow two parameter Weibull distribution, and the 50% survival probability was calculated based on the Weibull distribution equation below.

$$F(x) = \begin{cases} 1 - e^{-\left(\frac{x}{\lambda}\right)^k} & x \geq 0 \\ 0 & x < 0 \end{cases} \quad (2)$$

where x is fatigue life in logarithm, i.e., $\log_{10}(N_f)$, $k > 0$ is the shape parameter, and $\lambda > 0$ is the scale parameter. The fatigue life data in logarithm were ranked from the minimum value to the maximum value, and marked as $\log_{10}(N_{f,1})$, $\log_{10}(N_{f,2})$, ... $\log_{10}(N_{f,n})$, and the parameters in Equation (2) were determined by the best fitting of the distribution of the fatigue life in logarithm. The cumulative probability in logarithm of the fatigue life was calculated following the equation below.

$$F(\log_{10}(N_{f,i})) = \frac{i - 0.3}{n + 0.4} \quad (3)$$

where $i = 1, 2, 3, \ldots, n$, and n is the total number of specimens.

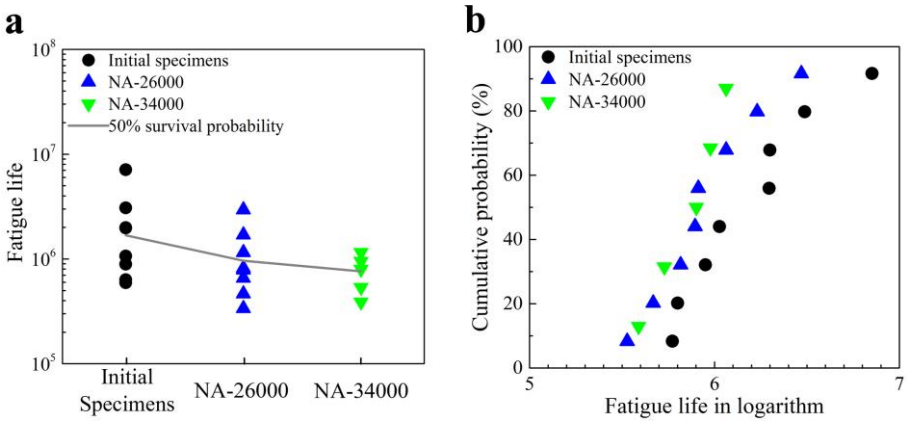

Figure 3. Fatigue life of 25CrMo4 specimens: (**a**) fatigue life versus natural-aging duration, (**b**) cumulative probability of fatigue life in logarithm after different natural-aging durations.

The 50% survival probability of the fatigue life in Figure 3a presents a consistent decreasing trend with the prolonged natural aging, and the values are reduced from 1.7×10^6 cycles of the initial specimens to 7.6×10^5 cycles of the specimens after NA-34000. The cumulative probability of the fatigue life in logarithm for the specimens after different natural-aging durations are shown in Figure 3b. It is seen that the probability of the initial specimens failed with a fatigue life $<1.0 \times 10^6$ cycles is <44%, but the probability of the specimens after NA-26000 and NA-34000 failed within this fatigue life range increases to >56% and >69%, respectively. It also confirms the trend that prolonged natural aging tends to reduce the fatigue life of 25CrMo4 steel.

SEM observation indicated that all the specimens failed from surface crack initiation, and the crack initiation was due to machined scratch or extrusion and intrusion under fatigue loading [30–32]. Figure 4 shows the fracture surfaces of the initial specimens and the specimens after NA-26000. For the initial specimens, most of the specimens failed from single-site crack initiation, as shown in Figure 4(a1), and only two specimens presented multi-site crack initiation as shown in Figure 4(b1). However, multi-site crack initiation became a dominant failure mode for the specimens after natural aging. After NA-26000, only two specimens failed from single-site crack initiation (Figure 4(c1)), four specimens had three crack initiation sites or above, and two specimens presented two crack initiation sites (Figure 4(d1)). The situation for the specimens after NA-34000 was similar. Two specimens had three crack initiation sites, two specimens had two crack initiation sites and only one specimen showed single-site crack initiation. Figure 5 shows the probability of single-site and multi-site crack initiations after different natural-aging durations. It is seen that the multi-site crack initiations tend to increase with increasing the aging time. The multi-side crack initiation mode after natural aging might be attributed to corrosion and hydrogen penetration in long-term storage. The content of Cr in the chemical composition is a little low for the 25CrMo4 steel, and it could not protect the steel from corrosion [33,34]. Based on the results in literature [16,35], corrosion and hydrogen penetration could occur in the rough surface and surface regions with inclusion in air. In this way, the loading capacity of the local regions could be reduced, and multi-site crack initiation could occur in these regions.

For a further investigation, the microstructure of 25CrMo4 steel after NA-34000 was observed by an optical microscope to understand its characteristics. As shown in Figure 6a, the microstructure includes coarse ferrite, pearlite, bainite and cementite-enriched area, and their distribution is nonuniform, especially for coarse ferrite and cementite-enriched area. The grain sizes of coarse ferrite reach 20~30 μm, and the coarse ferrite grains gather in local regions to form weak regions [36]. According to the precipitation of carbides due to natural aging reported in literature [15,17,18], the cementite-enriched area might be increased due to the carbide precipitation and gathering in the regions after the natural aging. Figure 6b shows the hardness of ferrite and cementite-enriched area, and the mean values between the two regions present significant difference. This might also have an adverse effect on the fatigue performance of 25CrMo4 steel.

3.2. Effect of Natural Aging on HCF of 30CrMnSiA Steel

Figure 7 shows the fatigue life data of 30CrMnSiA specimens after different natural-aging durations under the stress amplitude of 580 MPa. The fatigue lives of the initial specimens and the specimens after NA-8800 are close. However, the fatigue lives of the specimens after NA-20000 are lower than the initial specimens as a whole. Due to the less experimental data in Figure 7, the mean fatigue life in logarithm is used for the analysis of the natural-aging effect. The mean life of the initial specimen is 2.3×10^5 cycles, and it slightly decreases to 2.0×10^5 cycles after NA-8800. However, the mean life of the specimens after NA-20000 dramatically decreases to 9.8×10^4 cycles.. These results indicate that the effect of natural aging in a moderate period is not obvious for the fatigue performance of 30CrMnSiA steel, while the long-term natural aging is harmful.

Figure 8 shows the fracture surfaces of the 30CrMnSiA specimens in the initial state and after NA-8800. The initial specimens all failed from single-site crack initiation, as shown in Figure 8(a1), except one specimen presented two-site crack initiation. The fatigue cracks initiated from surface inclusion, as shown in Figure 8(a3). After NA-8800, single-site crack initiation was still a dominant failure mode (Figure 8(b1)), but two specimens failed from two-site crack initiation, as shown in Figure 8(c1). Similar to the initial specimens, the fatigue cracks of the specimens after NA-8800 also initiated from surface inclusion, as shown in Figure 8(b3,c2,c3). The crack initiation behavior of the specimens after NA-20000 was similar to those in the initial state and after NA-8800. Single-site crack initiation was a dominant failure mode, and one specimen failed from two-site crack initiation. It was seen that the natural aging did not change the dominant failure mode of single-site crack initiation, this performance was different from the 25CrMo4 steel reported in this paper.

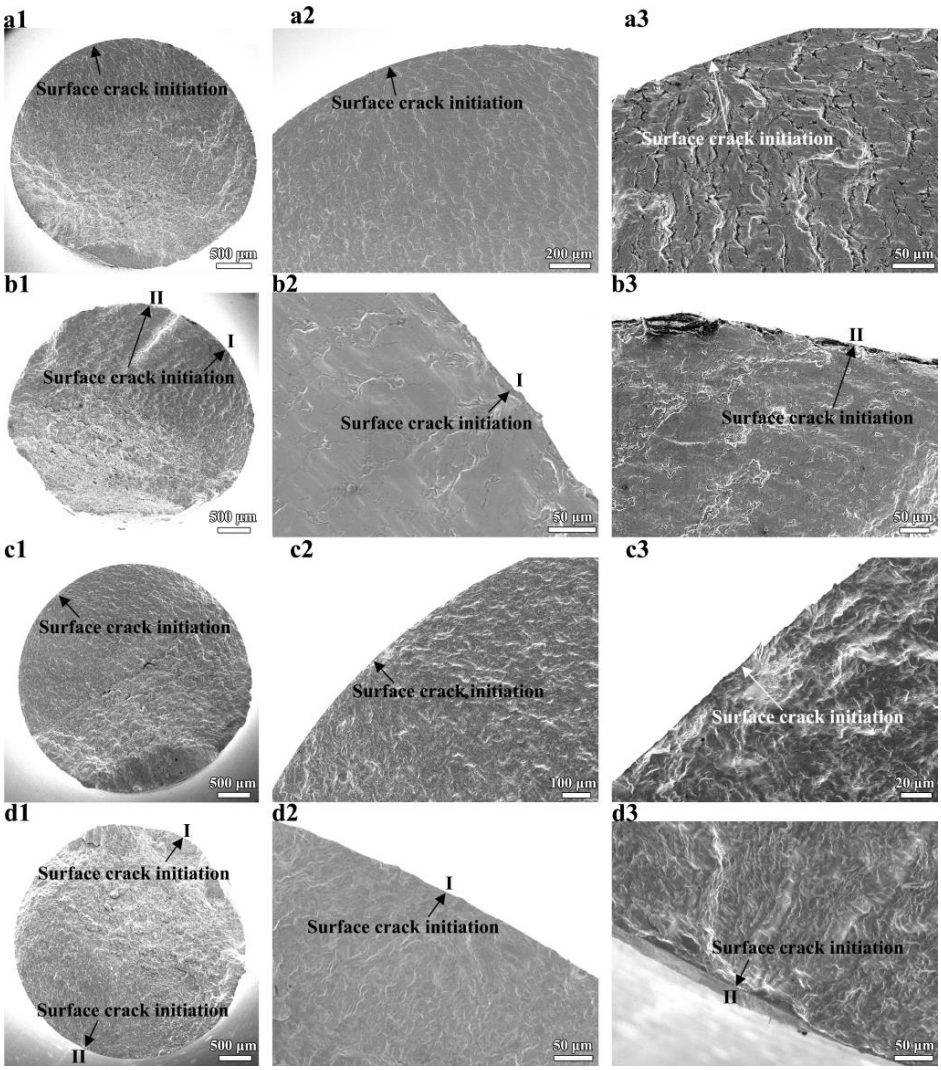

Figure 4. Fatigue fracture surfaces of 25CrMo4 specimens in the initial state and after NA-26000. (**a1**–**a3**) Initial specimen failed from single-site crack initiation: σ_a = 330 MPa, $N_f = 8.9 \times 10^5$ cycles; (**a2**,**a3**) are enlarged views of the crack initiation site. (**b1**–**b3**) Initial specimen failed from multi-site crack initiation: σ_a = 330 MPa, $N_f = 2.0 \times 10^5$ cycles; (**b2**,**b3**) are enlarged views of the two crack initiation sites. (**c1**–**c3**) Specimen after NA-26000 failed from single-site crack initiation: σ_a = 330 MPa, $N_f = 2.9 \times 10^5$ cycles; (**c2**,**c3**) are enlarged views of the crack initiation site. (**d1**–**d3**) Specimen after NA-26000 failed from multi-site crack initiation: σ_a = 330 MPa, $N_f = 1.2 \times 10^6$ cycles; (**d2**,**d3**) are enlarged views of the two crack initiation sites.

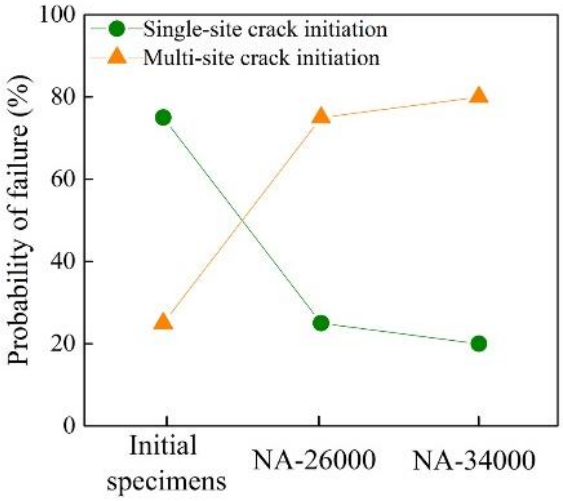

Figure 5. Probability of crack initiation modes for 25CrMo4 specimens after different natural-aging durations.

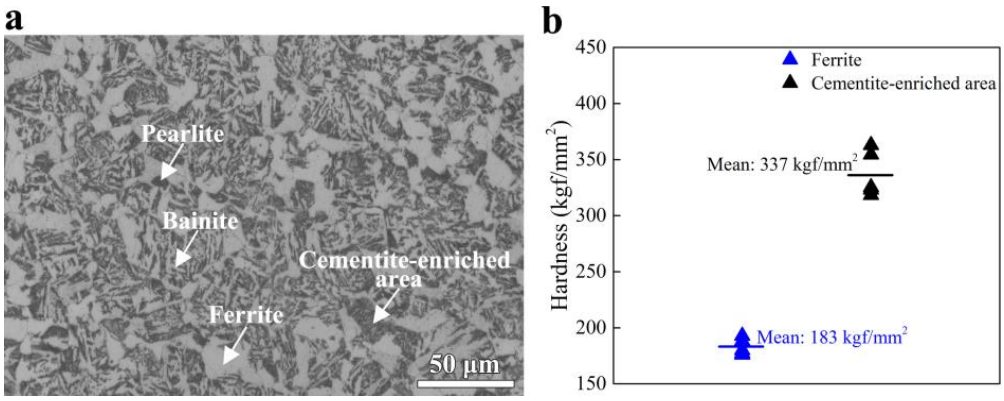

Figure 6. Microstructure characteristics of 25CrMo4 steel. (**a**) Microstructure image and (**b**) hardness of ferrite and cementite-enriched area in the microstructure.

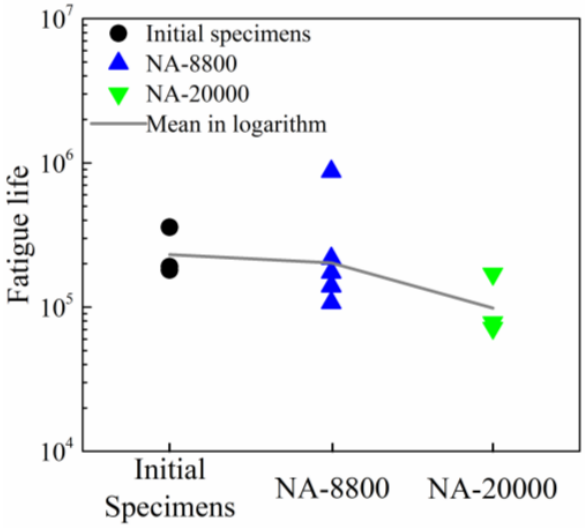

Figure 7. Fatigue life of 30CrMnSiA specimens versus natural-aging duration.

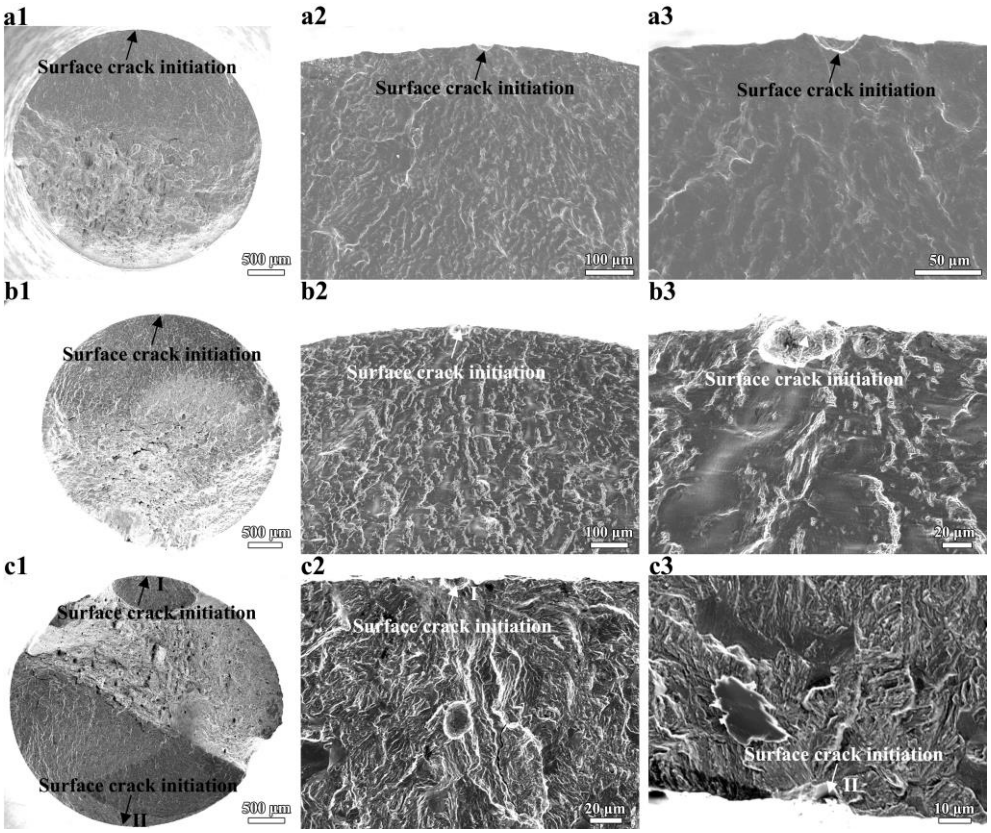

Figure 8. Fatigue fracture surfaces of 30CrMoSiA specimens in the initial state and after NA-8800: (**a1**–**a3**) Initial specimen failed from single-site crack initiation: σ_a = 580 MPa, $N_f = 1.8 \times 10^5$ cycles; (**a2**,**a3**) are enlarged views of the crack initiation site. (**b1**–**b3**) Specimen after NA-8800 failed from single-site crack initiation: σ_a = 580 MPa, $N_f = 1.4 \times 10^5$ cycles; (**b2**,**b3**) are enlarged views of the crack initiation site. (**c1**–**c3**) Specimen after NA-8800 failed from multi-site crack initiation: σ_a = 580 MPa, $N_f = 1.1 \times 10^5$ cycles; (**c2**,**c3**) are enlarged views of the two crack initiation sites.

Figure 9a,b show the microstructures of 30CrMnSiA steel observed by an optical microscope in the initial state and after NA-20000, respectively. Both images show tempered sorbite, and there is no obvious difference for the microstructure characteristic, which implies that the natural aging does not change the microstructure of the 30CrMnSiA steel. Therefore, the negative effect of NA-20000 might be attributed to the surface corrosion in the long-term storage of 30CrMnSiA specimens in air [16,37].

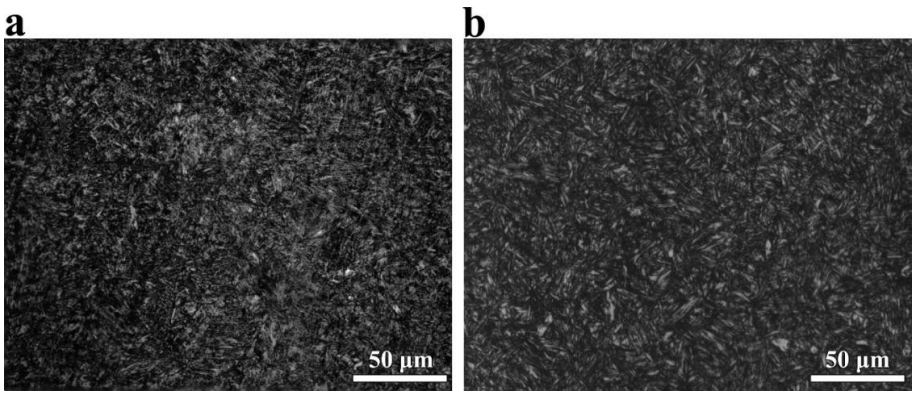

Figure 9. Microstructure of 30CrMnSiA steel. (**a**) Initial state; (**b**) after NA-20000.

The effect of natural aging is discussed here. The 25CrMo4 steel has a low Cr content of 0.54% in weight and has a nonuniform microstructure with coarse ferrite, pearlite, bainite and cementite-enriched area. The fatigue life of 25CrMo4 steel could be weakened after the natural aging of 26,000 h and above. The 30CrMnSiA steel has a low Cr content of 1.20% in weight and has a uniform tempered sorbite microstructure, and its fatigue performance keeps after the natural aging of 8800 h, but shows a decreasing trend after the natural aging of 20,000 h. Therefore, the negative effect of long-term natural aging on the fatigue behavior of 25CrMo4 steel and 30CrMnSiA steel might be attributed to their low Cr content and low resistance to corrosion as well as hydrogen penetration around rough surface and surface inclusion [33–35]. The corrosion in the local regions could accelerate the crack initiation [16,37] and reduce the fatigue life.

3.3. Effect of Discontinuous Loading on HCF of 25CrMo4 Steel

Figure 10a shows a comparison of fatigue life of 25CrMo4 specimens under continuous cyclic loading and discontinuous cyclic loading, and the fatigue life under discontinuous cyclic loading is slightly higher than that under continuous cyclic loading as a whole. Meanwhile, the cumulative probability of the fatigue life data is calculated based on Equation (3) to analyze the effect of discontinuous cyclic loading, as shown in Figure 10b. The specimens under continuous cyclic loading have a probability of 87% to fail at a fatigue life $<1.2 \times 10^6$ cycles, but for the specimens under discontinuous cyclic loading, the probability of the fatigue life within this range is only <50%. The result shows that the specimens under discontinuous cyclic loading tend to have a little longer fatigue life.

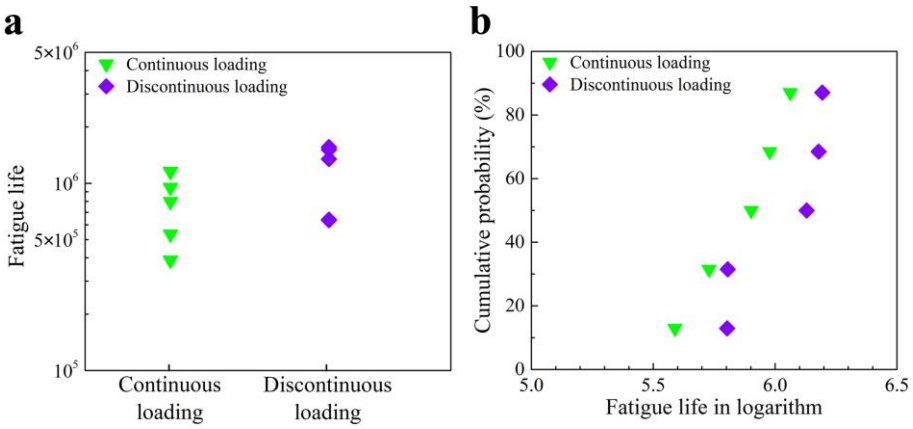

Figure 10. Comparison of fatigue life of 25CrMo4 specimens under continuous cyclic loading and discontinuous cyclic loading. (**a**) Fatigue life of the two loading conditions, (**b**) cumulative probability of fatigue life in logarithm.

Similar to the specimens under continuous cyclic loading, the specimens under discontinuous cyclic loading failed from single-site crack initiation or multi-site crack initiation, and all the cracks initiated from the specimen surface. Figure 11(a1–a3,b1–b3) show the SEM images of a single-site crack initiation and a multi-site crack initiation of the specimens under discontinuous cyclic loading, respectively. For the specimens under discontinuous cyclic loading, two specimens failed from single-site crack initiation and three specimens failed from multi-site crack initiation. The counts of multi-site crack initiation were close to those under continuous cyclic loading, indicating that the loading mode did not change the crack initiation mode.

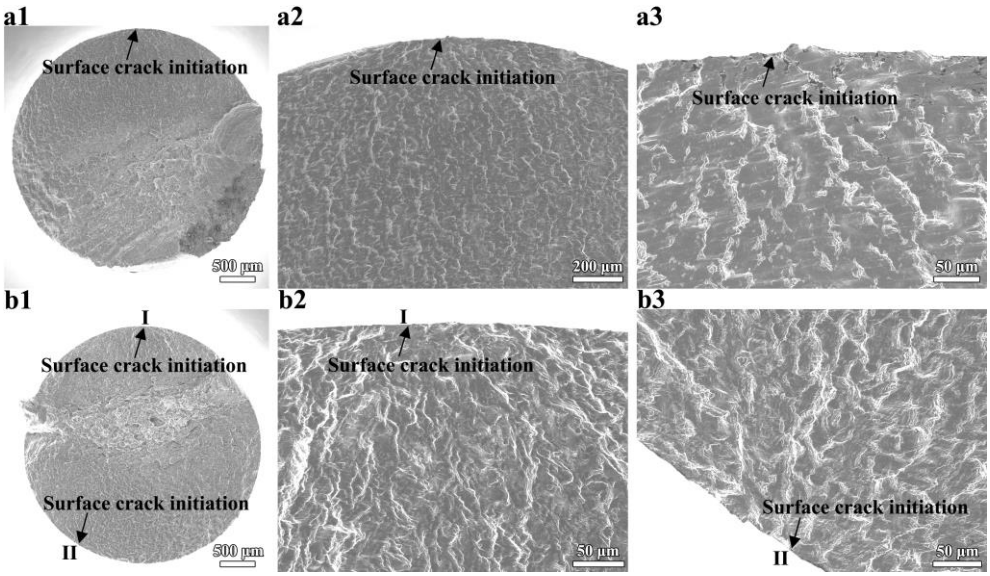

Figure 11. Fatigue fracture surfaces of 25CrMo4 specimens under discontinuous cyclic loading: (**a1**–**a3**) Specimen failed from single-site crack initiation: σ_a = 330 MPa, N_f = 1.6 × 10^6 cycles; (**a2**,**a3**) are enlarged views of the crack initiation site. (**b1**–**b3**) specimen failed from multi-site crack initiation: σ_a = 330 MPa, N_f = 6.4 × 10^5 cycles; (**b2**,**b3**) are enlarged views of the two crack initiation sites.

4. Conclusions

The effects of natural aging and discontinuous cyclic loading on HCF behavior of steels were studied by rotating bending fatigue tests. The main conclusions are as follows.

(1) The natural aging in a moderate period (e.g., less than 10,000 h) has no or negligible harmful influence on the fatigue life, while the long-term natural aging (e.g., more than 20,000 h) reduces the fatigue life of the 25CrMo4 steel and 30CrMnSiA steel. The reduction of the fatigue life should be due to the corrosion and the action of hydrogen at the specimen surface during the long-term natural aging.

(2) The effect of natural aging on the failure mechanism is related to the microstructure of materials. The dominant failure mode of 25CrMo4 specimens is switched from single-site crack initiation in the initial state to multi-site crack initiation after natural aging. While the dominant failure mode of 30CrMnSiA specimens after natural aging remains the single-site crack initiation.

(3) The discontinuous cyclic loading has no harmful influence on the fatigue life of the 25CrMo4 steel. It does not change the fatigue crack initiation mode. The specimens under continuous and discontinuous loadings both fail from single-site crack initiation or multi-site crack initiation at the specimen surface.

Author Contributions: G.L.: Methodology, Investigation, Writing—review & editing, Funding acquisition; J.L.: Investigation, Writing—review & editing; J.S.: Investigation, Writing—review & editing; C.S.: Conceptualization, Methodology, Investigation, Writing—review & editing, Funding acquisition, Supervision. All authors have read and agreed to the published version of the manuscript.

Funding: This research was funded by the support of the National Natural Science Foundation of China Basic Science Center for "Multiscale Problems in Nonlinear Mechanics" (11988102) and the fund of International Postdoctoral Exchange Fellowship Program (China).

Data Availability Statement: Data will be made available on request.

Conflicts of Interest: The authors declare that they have no known competing financial interests or personal relationships that could have appeared to influence the work reported in this paper.

References

1. Heinz, A.; Neumann, P. Crack initiation during high cycle fatigue of an austenitic steel. *Acta Metall. Mater.* **1990**, *38*, 1933–1940. [CrossRef]
2. Sonsino, C. Course of SN-curves especially in the high-cycle fatigue regime with regard to component design and safety. *Int. J. Fatigue* **2007**, *29*, 2246–2258. [CrossRef]
3. Wang, Y.; Wang, X.; Wu, S.; Yang, H.; Zhang, Z. High-cycle microscopic severe corrosion fatigue behavior and life prediction of 25crmo steel used in railway axles. *Metals* **2017**, *7*, 134. [CrossRef]
4. Giorgetti, A.; Millefanti, U.; La Battaglia, V.; Citti, P. Investigations of fatigue damage in a nitriding low-carbon bainitic steel for high-performance crankshaft. *Metals* **2022**, *12*, 2052. [CrossRef]
5. Krupp, U.; Giertler, A. Surface or internal fatigue crack initiation during VHCF of tempered martensitic and bainitic steels: Microstructure and frequency/strain rate dependency. *Metals* **2022**, *12*, 1815. [CrossRef]
6. Zhao, A.; Xie, J.; Sun, C.; Lei, Z.; Hong, Y. Effects of strength level and loading frequency on very-high-cycle fatigue behavior for a bearing steel. *Int. J. Fatigue* **2012**, *38*, 46–56. [CrossRef]
7. Sun, C.; Lei, Z.; Hong, Y. Effects of stress ratio on crack growth rate and fatigue strength for high cycle and very-high-cycle fatigue of metallic materials. *Mech. Mater.* **2014**, *69*, 227–236. [CrossRef]
8. Huang, J.; Yeh, J.; Jeng, S.; Chen, C.; Kuo, R. High-cycle fatigue behavior of type 316L stainless steel. *Mater. Trans.* **2006**, *47*, 409–417. [CrossRef]
9. Kwon, J.; Woo, S.; Lee, Y.; Park, J.; Park, Y. Effects of thermal aging on the low cycle fatigue behavior of austenitic–ferritic duplex cast stainless steel. *Nucl. Eng. Des.* **2001**, *206*, 35–44. [CrossRef]
10. Llanes, L.; Mateo, A.; Violan, P.; Mendez, J.; Anglada, M. On the high cycle fatigue behavior of duplex stainless steels: Influence of thermal aging. *Mater. Sci. Eng. A* **1997**, *234*, 850–852. [CrossRef]
11. Pérez-Mora, R.; Palin-Luc, T.; Bathias, C.; Paris, P. Very high cycle fatigue of a high strength steel under sea water corrosion: A strong corrosion and mechanical damage coupling. *Int. J. Fatigue* **2015**, *74*, 156–165. [CrossRef]
12. El May, M.; Palin-Luc, T.; Saintier, N.; Devos, O. Effect of corrosion on the high cycle fatigue strength of martensitic stainless steel X12CrNiMoV12-3. *Int. J. Fatigue* **2013**, *47*, 330–339. [CrossRef]
13. Gao, J.; Pan, X.; Han, J.; Zhu, S.; Liao, D.; Li, Y.; Dai, G. Influence of artificial defects on fatigue strength of induction hardened S38C axles. *Int. J. Fatigue* **2020**, *139*, 105746. [CrossRef]
14. Murakami, Y.; Endo, M. Effects of defects, inclusions and inhomogeneities on fatigue strength. *Int. J. Fatigue* **1994**, *16*, 163–182. [CrossRef]
15. Li, G.; Ke, L.; Peng, W.; Ren, X.; Sun, C. Effects of natural aging and variable loading on very high cycle fatigue behavior of a bearing steel GCr15. *Theor. Appl. Fract. Mech.* **2022**, *119*, 103360. [CrossRef]
16. Botvina, L.; Petrova, I.; Gadolina, I.; Levin, V.; Demina, Y.; Soldatenkov, A.; T'utin, M. High-cycle fatigue failure of low-carbon steel after long-term aging. *Inorg. Mater.* **2010**, *46*, 1570–1577. [CrossRef]
17. Chang, P. Temper-aging of continuously annealed low carbon dual phase steel. *Metall. Trans. A* **1984**, *15*, 73–86. [CrossRef]
18. Zamani, M.; Mirzadeh, H.; Maleki, M. Enhancement of mechanical properties of low carbon dual phase steel via natural aging. *Mater. Sci. Eng. A* **2018**, *734*, 178–183. [CrossRef]
19. Tai, C.; Tai, P.; Hsiao, T.; Chiu, P.; Tseng, C.; Tsao, T.; Chung, T.; Yang, Y.; Chen, C.; Wang, S.; et al. Effect of natural ageing on subsequent artificial ageing of aa7075 aluminum alloy. *Metals* **2022**, *12*, 1766. [CrossRef]
20. Fritsch, S.; Wagner, M. On the effect of natural aging prior to low temperature ECAP of a high-strength aluminum alloy. *Metals* **2018**, *8*, 63. [CrossRef]
21. Cui, Z.; Jiang, H.; Zhang, D.; Song, Y.; Yan, D.; Rong, L. Effect of natural aging on precipitation strengthening behaviors in al-mg-si alloy. *Metals* **2022**, *12*, 470. [CrossRef]
22. Park, M.; So, H.; Kim, K.; Byeon, J.; Kang, L. Natural Aging Effect of Al-20Zn-3Cu alloy on mechanical properties and its relation to microstructural change. *Metals* **2021**, *11*, 1485. [CrossRef]
23. Sun, C.; Li, Y.; Xu, K.; Xu, B. Effects of intermittent loading time and stress ratio on dwell fatigue behavior of titanium alloy Ti-6Al-4V ELI used in deep-sea submersibles. *J. Mater. Sci. Technol.* **2021**, *77*, 223–236. [CrossRef]
24. Peng, W.; Zhang, Y.; Qiu, B.; Xue, H. A brief review of the application and problems in ultrasonic fatigue testing. *AASRI Procedia* **2012**, *2*, 127–133. [CrossRef]
25. Sun, C.; Song, Q.; Hu, Y.; Wei, Y. Effects of intermittent loading on fatigue life of a high strength steel in very high cycle fatigue regime. *Int. J. Fatigue* **2018**, *117*, 9–12. [CrossRef]
26. Murtaza, G.; Akid, R. Corrosion fatigue short crack growth behaviour in a high strength steel. *Int. J. Fatigue* **1996**, *18*, 557–566. [CrossRef]
27. *GB/T4337-2015*; Metallic Materials-Fatigue Testing-Rotating Bar Bending Method. Standardization Administration of China: Beijing, China, 2015.
28. Goodno, B.; Gere, J. *Mechanics of Materials*; Cengage Learning: Stamford, CT, USA, 2020.
29. Sun, C.; Song, Q. A method for predicting the effects of specimen geometry and loading condition on fatigue strength. *Metals* **2018**, *8*, 811. [CrossRef]
30. Hu, Y.; Wu, S.; Withers, P.; Cao, H.; Chen, P.; Zhang, Y.; Shen, Z.; Vojtek, T.; Hutar, P. Corrosion fatigue lifetime assessment of high-speed railway axle EA4T steel with artificial scratch. *Eng. Fract. Mech.* **2021**, *245*, 107588. [CrossRef]

31. Xu, Z.; Wu, S.; Wang, X. Fatigue evaluation for high-speed railway axles with surface scratch. *Int. J. Fatigue* **2019**, *123*, 79–86. [CrossRef]
32. Polák, J.; Mazánová, V.; Heczko, M.; Petráš, R.; Kuběna, I.; Casalena, L.; Man, J. The role of extrusions and intrusions in fatigue crack initiation. *Eng. Fract. Mech.* **2017**, *185*, 46–60. [CrossRef]
33. Dugstad, A.; Hemmer, H.; Seiersten, M. Effect of steel microstructure on corrosion rate and protective iron carbonate film formation. *Corrosion* **2001**, *57*, 369–378. [CrossRef]
34. Kamimura, T.; Stratmann, M. The influence of chromium on the atmospheric corrosion of steel. *Corros. Sci.* **2001**, *43*, 429–447. [CrossRef]
35. Murakami, Y.; Nomoto, T.; Ueda, T. Factors influencing the mechanism of superlong fatigue failure in steels. *Fatigue Fract. Eng. Mater. Struct.* **1999**, *22*, 581–590. [CrossRef]
36. Hijazi, F.; Kar, J.; Pavan, A.; Singh, K.; Kumar, P.; Jayaram, V. Application of bending creep for examining effect of service conditions on creep response of steel. *Mater. Sci. Eng. A* **2019**, *766*, 138398. [CrossRef]
37. Miller, K.; O' donnell, W. The fatigue limit and its elimination. *Fatigue Fract. Eng. Mater. Struct.* **1999**, *22*, 545–557. [CrossRef]